7

Study on Substitution Effect of $Bi_4Ti_3O_{12}$ Ferroelectric Thin Films

Jianjun Li[1,2], Ping Li[1] and Jun Yu[2]
[1]*University of Electronic Science and Technology of China*
[2]*Huazhong University of Science and Technology*
China

1. Introduction

Nowadays, ferroelectric thin films have attracted considerable attention because of their potential uses in device applications, such as sensors, micro electro-mechanical system (MEMS) and nonvolatile ferroelectric random access memory (NvFRAM) especially (Scott & Paz De Araujo, 1989; Paz De Araujo et al., 1995; Park et al. 1999). Lead zirconate titanate [$PbZr_xTi_{1-x}O_3$ (PZT)] ferroelectric thin film is an early material for NvFRAM. PZT and related ferroelectric thin films, which are most widely investigated, usually have high remanent polarization (P_r). However, they are generally suffered from a serious degradation of ferroelectric properties with polarity switching, when they are deposited on platinum electrodes.

Bismuth-layered perovskite ferroelectric thin films, with the characteristics of fast switching speed, high fatigue resistance with metal electrodes, and good retention, have attracted much attention. Bismuth titanate [$Bi_4Ti_3O_{12}$ (BIT)] is known to be a typical kind of layer-structured ferroelectrics with a general formula $(Bi_2O_2)^{2+}(A_{m-1}B_mO_{3m+1})^{2-}$. Its crystal structure is characterized by three layers of TiO_6 octahedrons regulary interleaved by $(Bi_2O_2)^{2+}$ layers. At room temperature the symmetry of BIT is monoclinic structure with the space group B1a1, while it can be considered as orthorhombic structure with the lattice constant of the *c* axis (c = 3.2843 nm), which is considerably larger than that of the other two axis (a = 0.5445 nm, b = 0.5411 nm). The BIT has a spontaneous polarization in the *a*-*c* plane and exhibits two independently reversible components along the *c* and *a* axis (Takenaka & Sanaka, 1980; Ramesh et al., 1990). It shows spontaneous polarization values of 4 and 50 μC/cm² along the *c* and *a* axis respectively. The ferroelectric properties of these bismuth layer-structured thin films are mostly influenced by the orientation of the films (Simoes et al., 2006). The BIT thin film is highly *c*-axis oriented, thus its spontaneous polarization is much lower than that for *a*-axis oriented (Fuierer & Li, 2002). For applications in NvFRAM devices, ferroelectric materials should have high remanent polarization, low coercive field (E_c), low fatigue rate and low leakage current density. However, BIT thin film has much lower values of switching polarization and suffers from poor fatigue endurance and high leakage current as a result of the internal defects (Uchida et al., 2002). Numerous works have been made to substitute BIT thin film with proper ions to optimize the ferroelectric properties.

In recent years, it was reported that some *A*-site or *B*-site substituted BIT showed large remanent polarizations. In the case of *A*-site substitution in BIT, La-substituted BIT

[$Bi_{3.25}La_{0.75}Ti_3O_{12}$ (BLT)] films exhibited enhanced P_r of 12 μC/cm² with high fatigue resistance, which make them applicable to direct commercialization (Chon et al., 2002). Other lanthanides ions, such as Nd^{3+}, Pr^{3+}, Sm^{3+}, etc. result in similar results (Watanabe et al., 2005; Chon et al., 2003; Chen et al., 2004). In the case of *B*-site substitution in BIT, some donor ions such as V^{5+}, Nd^{5+}, W^{6+}, could effectively decrease the space charge density resulting in the improvement of the ferroelectric properties (Kim et al., 2002; Wang & Ishiwara, 2003). For further improvement of the ferroelectric properties, *A* and *B*-site cosubstitution by various ions should be considered because the properties of BIT based materials strongly depend on species of the substituent ions.

In this chapter, we first summarized the researches on the effect of *A*-site or/and *B*-site substitution on microstructures and properties of $Bi_4Ti_3O_{12}$ ferroelectric thin films. Then La/V substituted BIT thin films were deposited by sol-gel method, and the effect of substitution of La^{3+} and V^{5+} on structural and electrical properties of the BIT thin film was investigated.

2. *A*-site or *B*-site substitution

2.1 *A*-site substitution

The properties of different *A*-site substituted BIT thin films were summarized in Table 1. La-substituted BIT (BLT) films exhibited large P_r and low E_c with high fatigue resistance, and BLT thin film has been already applied in commercial NvFRAM product in all *A*-site substituted BIT thin films.

Substitution Ion	Content	Orientation	$2P_r$ (μC/cm²)	$2E_c$ (kV/cm)	Fatigue Endurance	References
La	0.75	random	24	100	3×10^{10}	Park et al. 1999
Nd	0.85	random	63.6	260	3×10^{10}	Hou et al. 2005
		c	103	190	6.5×10^{10}	Chon et al. 2002
		(104)	40	100	10^9	Garg et al. 2003
Pr	0.3	*a*	92	100	-	Matsuda et al. 2003
	0.85	*c*	40	-	4.5×10^{10}	Chom et al. 2003
	0.9	random	60	104	-	Chen et al. 2004
Sm	0.85	c	49	113	4.5×10^{10}	Chon et al. 2001
Gd	0.6	random	49.6	249	1.45×10^{10}	Kim et al. 2005

Table 1. Summary of the properties of different *A*-site substituted BIT thin films

Yau et al. (Yau et al. 2005) reported the mechanism of polarization enhancement in La-substituted BIT thin films. Independently controlling processing temperature or La substitution could adjust the orientation and enhance the P_r. Increasing La substitution decreased *c* orientation but increased P_r. The lattice paraments *a*, *b* and *c* of $Bi_{4-x}La_xTi_3O_{12}$ films increase monotonously with La content *x* from *x*=0-0.6. The fitted lines (assumed for *x*>0.6), with different positive slopes, indicated different enlargements in *a*, *b* and *c* and an increase in cell volume. The increase in the *a*, *b* and *c* lattice paramenters approached single crystal values with increasing *x*, which also lowered the orthorhombic distortion, i.e., $2(a-b)/(a+b)$. This strongly suggested that the relaxations of structural distortion and strain arise from the La substitution, which also enhanced P_r.
Lee et al. (Lee et al. 2002) reported correlation between internal stress and ferroelectric fatigeue in La-substituted BIT films. When the La content exceeded *x*=0.25, there was little change in the chemical stability of elements. Chemical stability of oxygen ions alone could not fully explain the effect of La substitution on fatigue. The decrease of the strain was saturated at a composition of *x*=0.75, and films showed fatigue-free characteristics with this composition. Thus, internal strain as well as chemical stability of ions play a significant role in the fatigue behavior of BLT films.

2.2 *B*-site substitution

The properties of different *B*-site substituted BIT thin films were summarized in Table 2 (Choi et al., 2004).

Substitution Ion	c-axis orientation fraction (%)	$2P_r$ (calc.) ($\mu C/cm^2$)	$2P_r$ (meas.) ($\mu C/cm^2$)
-	97.6	8.6	11.1
V	83.6	11.3	11.9
W	65.2	14.7	14.3
Nb	29.1	21.5	22.9

Table 2. Summary of the properties of different *B*-site substituted BIT thin films

Either *A*-site or *B*-site substitution can improve remanent polarization of BIT thin film, but the mechanism is different with each other, and the effect of *A*-site substitution is prominent. For *A*-site substitution, there is a highly asymmetric double-well potential at TiO_6 octahedro unit adjacent to the interleaving Bi_2O_2 layer along the *c* axis, and it results in the development of remanent polarization along the *c* axis. For *B*-site substitution, the decreasing *c*-axis orientation results in the development of remanent polarization. Simultaneously, the role of *A*-site substitution is to suppress the *A*-site vacancies accompanied with oxygen vacancies which act as space charge. And the role of *B*-site substitution is the compensation for the defects, which cause a fatigue phenomenon and strong domain pinning. For further improvement of the ferroelectric properties, *A* and *B*-site cosubstitution by various ions should be considered because the properties of BIT based materials strongly depend on species of the substituent ions.

3. La/V substitution

3.1 Experimental

The BIT, $Bi_{3.25}La_{0.75}Ti_3O_{12}$ (BLT), $Bi_{4-x/3}Ti_{3-x}V_xO_{12}$ (BTV) and La^{3+}/V^{5+} cosubstituted BIT [$Bi_{3.25-x/3}La_{0.75}Ti_{3-x}V_xO_{12}$ (BLTV)] thin films were prepared on the $Pt/TiO_2/SiO_2/p$-Si(100) substrates by sol-gel processes. The sol-gel method is one of the chemical solution deposition (CSD) methods, which is commonly used as a fabrication method for thin films. The important advantages of sol-gel method are high purity, good homogeneity, lower processing temperatures, precise composition control of the deposition of multicomponent compoudns, versatile shaping, and deposition with simple and cheap apparatus.

The precursor solution for these films were prepared from Bismuth nitrate [$Bi(NO_3)_3 \bullet 5H_2O$], lanthanum nitrate [$La(NO_3)_3 \bullet xH_2O$], titanium butoxide [$Ti(OC_4H_9)_4$] and vanadium oxytripropoxide [$VO(C_3H_7O)_3$]. The bismuth nitrate and lanthanum nitrate were dissolved in 2-methoxyethanol at room temperature to reach clear solution. Titanium butoxide and vanadium oxytripropoxide were stabilized by acetylacetone at room temperature, which was also act as the stabilizer. These related solutions were mixed, then sonicated and refluxed to dissolve the solutes sufficiently and improved the stability of the solutions. The final concentration in these mixed solutions was adjusted to 0.1 mol/L, and the solutions were aged in vessels for 24 h to get the BIT, BLT, BTV and BLTV precursors. A 10 mol% excess amount of bisumth nitrate was used to compensate Bi evaporation during the heat treatment. The precursor solutions were spin-coated on the $Pt/TiO_2/SiO_2/p$-Si(100) substrates at 3700rpm for 30 s. Then the sol films were dried at 300°C for 5 min and pyrolyzed at 400°C for 10 min to remove residual organic compounds. These processes were repeated six times to achieve the desired film thickness. Then the films were annealed at 750°C for 30 min under air ambient in a horizontal quartz-tube furnace to produce the layered-perovskite phase.

The phase identification, crystalline orientation, and degree of crystallinity of the prepared films were studied by a χ' Pert PRO X-ray diffractometer (PANalytical, B V Co., Holland) with Cu-Ka radiation at 40 kV. The surface and cross-section morphologies were investigated using a Sirion 200 field-emission scanning electron microscope (FEI Co., Holland). The local microstructure and local symmetry of the films were also characterized by Raman spectroscopy (LabRam HR800, Horiba Jobin Yvon Co., France). The Raman measurements were performed at room temperature using the 514.5 nm line of an argon ion laser as the excitation source. Pt top electrodes with an area of about 7×10^{-4} cm^2 were deposited by means of sputtering using a shadow mask for electrical measurements. The polarization-voltage (*P-V*) hysteresis loops and fatigue of the films were measured by using a RT66A ferroelectric test system (Radiant Technology Inc., USA), and the leakage current behaviors of the films were analyzed using a Keithley 2400 sourceMeter/High Resistance Meter (Keithley Instruments Inc., USA) with a staircase dc-bias mode and appropriate delay time at each voltage step.

3.2 The effect of La/V substitution

The XRD patterns of the BIT, BLT, BTV (x=0.03) BLTV (x=0.03) thin films deposited on the $Pt/TiO_2/SiO_2/p$-Si(100) substrates are shown in Fig. 1. All the diffraction peaks of these film samples can be indexed according to the reference pattern of $Bi_4Ti_3O_{12}$ powder [BIT, JCPDS (Joint Committee on Powder Diffraction Standards) 35-795]. The good agreement in XRD peaks of the BLT, BTV and BLTV films with those of BIT indicates that the lattice structure

of these films are similar to that of BIT. It can be seen that all the films are the single phase of layer-structured perovskite and no pyrochlore phase. The BIT film exhibits a high *c*-axis orientation with the (*00l*) peak being of highest intensities, while the BLTV film exhibits a highly random orientation with the (117) peak being of highest intensity. In order to determine the degree of preferred orientation, the volume fraction of *c*-axis-oriented grains in a film sample is defined as

$$\alpha_{(00l)} = \Sigma(I_{00n} / I^*_{00n}) / \Sigma(I_{hkl} / I^*_{hkl}) \quad (1)$$

Where I_{hkl} is the measured intensity of (*hkl*) for the films, I^*_{hkl} is the intensity for powders, and n is the number of reflections (Lu et al., 2005; Bae et al., 2005). The α values obtained for the BIT, BLT, BTV BLTV films corresponding to Fig. 1 are 76.4, 46.1, 52.5 and 24.4% respectively. The BIT film shows *c*-axis preferred orientation, other films show random orientation.

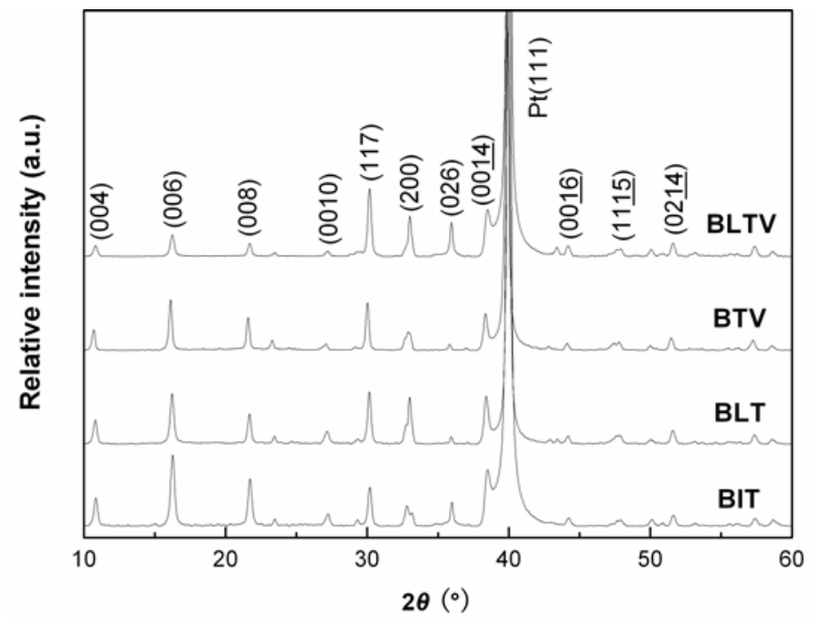

Fig. 1. XRD patterns of the BIT, BLT, BTV and BLTV thin films deposited on the Pt/TiO_2/SiO_2/p-Si(100) substrates

The BIT film has a strong tabular habit with the growth of *c*-axis orientation, for the energy of the (*00l*) surfaces is lower and consequently the (*h00*) and (*0k0*) faces grow more rapidly. Yau et al. (Yau et al. 2005) reported that, for La-substituted BIT thin films ($Bi_{4-x}La_xTi_3O_{12}$), the degree of *c*-axis orientation decreases with the increase of La content *x* (Yau et al., 2005). Choi et al. reported that, for *B*-site(V^{5+}, W^{6+}, Nb^{5+}) substituted BIT thin films, the degree of *c*-axis orientation decreases greatly with different donor ions substitution (Choi et al., 2004). The substitution may break down the Ti-O chains due to the differences in the electron affinites, which results in the clusters in the precursor favoring the growth of non-*c*-axis orientation. Thus, the BLT, BTV and BLTV thin films with substitition exhibit less highly *c*-axis oriented than the typical unsubstituted BIT thin film, and the result suggests that substitution has an important effect on the orientation of the BIT films.

The lattice constants of the four different film samples are also influenced by the substitution. The lattice constans have been calculated from the XRD patterns and listed in

Table 3. The lattice constant, *a*, decreases and *b* increases as La^{3+} is substituted, while a increases and *b* decreases as V^{5+} is substituted. The orthorhombicity could reflect the variation in the lattice constants, which is defined as $2(a-b)/(a+b)$. The variation of orthorhombicity agrees well with those reported in the literature for La-substituted $Bi_4Ti_3O_{12}$. The decrease of orthorhombicity for the BLT film suggests relaxation of the structural distortion, while the increase for the BTV and BLTV films suggests a increase of the structural distortion and a decrease of the symmetry.

	a (nm)	*b* (nm)	*c* (nm)	$2(a-b)/(a+b)$
BIT	0.5421	0.5391	3.2763	5.55×10^{-3}
BLT	0.5419	0.5392	3.2776	4.96×10^{-3}
BTV	0.5432	0.5386	3.2731	8.50×10^{-3}
BLTV	0.5426	0.5388	3.2756	7.03×10^{-3}

Table 3. Lattice constants and orthorhombicity for the BIT, BLT, BTV and BLTV thin films

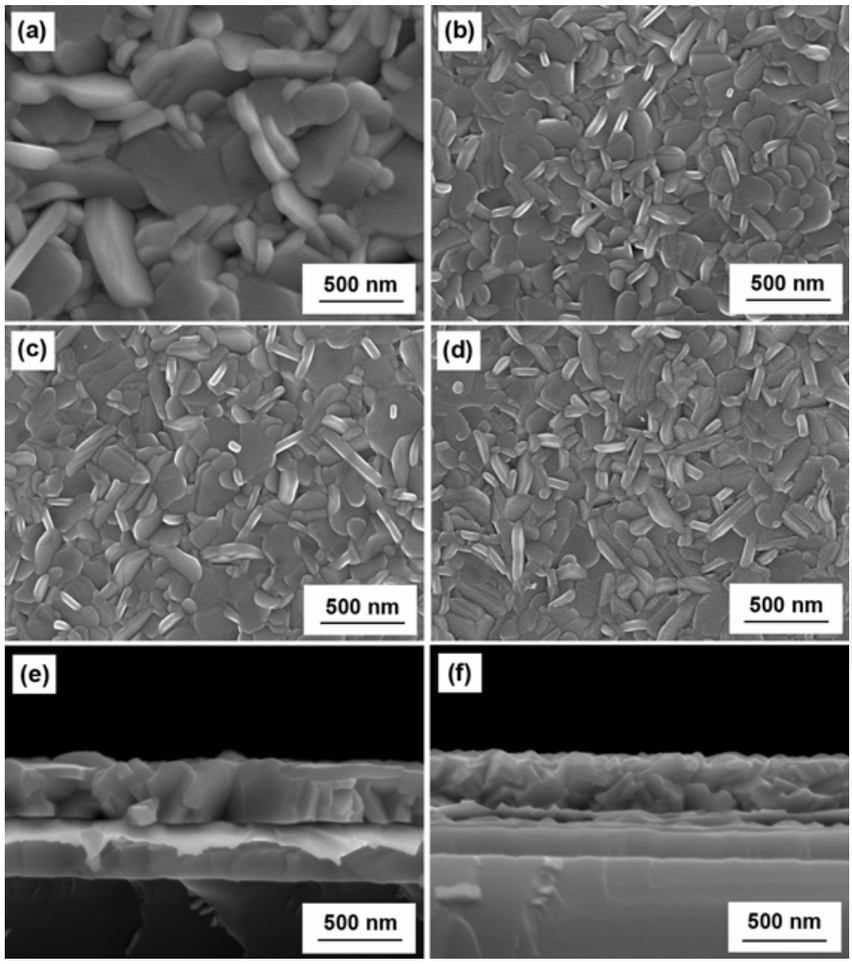

Fig. 2. FE-SEM surface morphologies of the (a) BIT, (b) BLT, (c) BTV and (d) BLTV thin films, and the cross-section micrographs of the (e) BIT and (f) BLTV thin films

Figure 2 shows the field-emission scanning electron microscopy (FE-SEM) surface and cross-section morphologies of these thin films. All the films show dense microstructure without any crack. The thickness of the films is about 360 nm by the cross-section view. From the surface morphologies, it can be seen that the BLTV film is mainly composed of fine rod-like grains with small sizes about 80-160 nm in Fig. 2(d), while the BIT film is mainly composed of large or small plate-like grains with sizes up to 200-500 nm in Fig. 2(a). And it also can been found from the cross-section micrographs, the rod-like grains for the BLTV film slant toward to the film surface in Fig. 2(f), while the large columnar grains for the BIT film are vertical to the film surface in Fig. 2(e). The rod-like grains increase and plate-like grains decrease in the BIT films after substitution of La^{3+} or V^{5+}, and also the size of plate-like grains decreases. For BIT based films, the rod-like grains are related to the growth of random orientation and the plate-like grains are related to the growth of *c*-axis orientation (Lee et al., 2002; Li et al.,2007). In Fig. 1, we can see that the full-width at falf-maximum (FWHM) of the (*00l*) peak decreases after substitution of La^{3+} or V^{5+}, which indicates the restricted growth of (*00l*)-oriented grains. So the results of FE-SEM surface and cross-section morphologies agree with those of the XRD patterns discussed above.

Raman scattering is a powerful probe in studying complex-structured materials because it is highly sensitive to local microstructure and symmetry. The Raman spectra for these films were investigated in the Raman frequency shift range of 100-1000 cm^{-1} as presented in Fig. 3. For bismuth layer-structured ferroelectrics (BLSFs), their phonon modes can generally be classified into two categories: low frequency modes below 200 cm^{-1} and high frequency modes above 200 cm^{-1} (Shulman et al., 2000). The low frequency modes below 200 cm^{-1} are related to large atomic masses, which reflect the vibration of Bi^{3+} ions in $(Bi_2O_2)^{2+}$ layer and *A*-Site Bi^{3+} ions. The high frequency modes above 200 cm-1 reflect the vibration of Ti^{4+} and TiO_6 octahedron. The phonon modes at 118 and 147 cm^{-1} reflect the vibration of *A*-site Bi^{3+} ions in layer-structured perovskite. These modes shift to higher frequencies in the BLT and BLTV films after *A*-site La^{3+} substitution, but almost remain unchanged in the BTV film after *B*-site V^{5+} substitution, which suggests the *B*-site V^{5+} substitution has not affected the *A*-site Bi^{3+} ion. The average masses of La/Bi decrease for La atomic mass is lower than Bi atomic mass (M_{La}/M_{Bi}=139/208), so the related modes show high-frequency shift, which also indicates *A*-site Bi^{3+} ions in BIT film are partly substituted for La^{3+}.

The 231 and 270 cm^{-1} modes are considered to reflect the distortion modes of TiO_6 octahedron. The 231 cm^{-1} mode is Raman inactive when the symmetry of the TiO_6 octahedron is O_h, but it becomes Raman active when distortion occurs in TiO_6 octahedron. The disappearance of the 231 cm^{-1} mode and low-frequency shift of 270 cm^{-1} mode for the BLT film could be explained by a decrease in distortion of TiO_6 due to the influence of La^{3+} ions substitution which may lower the corresponding binding strength and decrease the Raman shift (Zhu et al., 2005). And it is consistent with the decrease of orthorhombicity for the BLT film. While in B-site V^{5+} substituted BTV film, the 231 cm^{-1} mode almost remains unchanged and 270 cm^{-1} mode shifts to a slightly higher frequency. These results suggest that the *A*-site La^{3+} substitution has influenced the *B*-site Ti^{4+} ions in TiO_6 octahedron.

The 537 and 565 cm^{-1} modes are attributed to a combination of stretching and bending of TiO_6 octahedron in BIT. According to references, *A*-site La^{3+} substitution leads to structural disorder and in turn broadens the line of these two modes, thus resulting in the mode at 557 cm^{-1} in the BLT and BLTV films (Wu et al., 2001). The only *B*-site V^{5+} substitution in the BTV film does not affect these two original modes greatly with both shifting to slightly higher

frequencies. Thus the variation of the mode frequencies at 537, 557 and 565 cm^{-1} also implies that the A-site La^{3+} substitution exerts influence on Ti^{4+} ions in B sites of the BIT thin film.

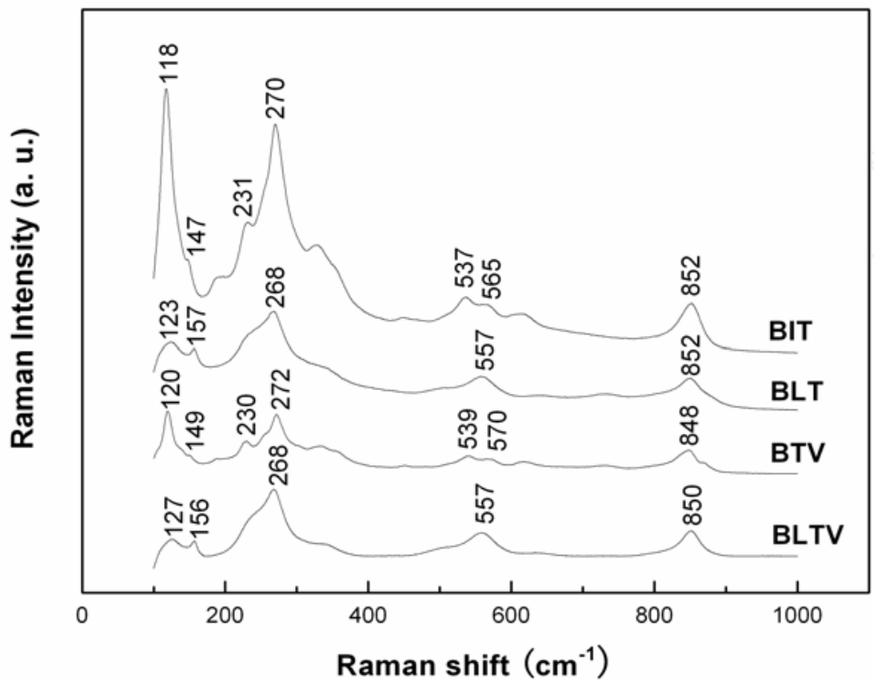

Fig. 3. Raman spectra of the BIT, BLT, BTV and BLTV thin films

The 852 cm^{-1} mode is a pure stretching of TiO_6 octahedron (Yau et al., 2005; Mao et al., 2006). The *A*-site La^{3+} substitution in the BLT film hardly affects the mode, while the *B*-site V^{5+} substitution in the BTV film results in its significant low-frequency shift, indicating that the V^{5+} is entering into the lattice replacing the Ti^{4+} in *B* site and a decrease in O_h symmetry of TiO_6 octahedron, which is consistent with the increase of orthorhombicity for the BTV film. The wave number of the mode of the BLTV film is between the corresponding one of the BLT and BTV films, which should be attributed to the effects of cosubstitution of La^{3+} and V^{5+} in *A* and *B* sites, respectively. On the other hand, for the BLTV film, since V^{5+} is electronically more active than Ti^{4+}, and there is a little asymmetry of TiO_6, a increase in Ti-O hybridization is implied.

Figure 4 shows the *P*-*V* curves of the BIT, BLT, BTV and BLTV thin film capacitors at a voltage of 12 V. The only *B*-site V^{5+} substitution improves the ferroelectric properties of BIT film slightly. The BLT and BLTV films show well-saturated hystersis loops. The measured values of $2P_r$ and $2E_c$ are 15.6 μC/cm² and 248 kV/cm for the BIT film, 37.6 μC/cm² and 226 kV/cm for the BLT film, 21.6 μC/cm² and 188 kV/cm for the BTV film, 50.8 μC/cm² and 194 kV/cm for the BLTV film, respectively. For *A*-site substituted BIT film, the E_c usually varys slightly, while for *B*-site substituted BIT film, the E_c becomes smaller (Wang & Ishiwara, 2002). All these substitutions can improve the P_r value for the BIT film, and the BLTV film has the largest P_r with smaller E_c among these films. On one hand, the spontaneous polarization of BIT along the *c*-axis is know to be much smaller than that along the *a*-axis. From this viewpoint, randomly oriented films are considered to be more favorable than *c*-axis oriented films. Therefore the randomly oriented BLTV and BLT films have a more

suitable orientation in comparison with other film samples for achieving large P_r. And the BLTV film gets the largest P_r for its least degree of *c*-axis orientation. On the other hand, as hybridization is essential to ferroelectricity, the increase of hybridization may increase the polarization (Cohen, 1992). Thus the increase of Ti-O hybridization inside TiO_6 of the BLTV film results in its excellent ferroelectric properties.

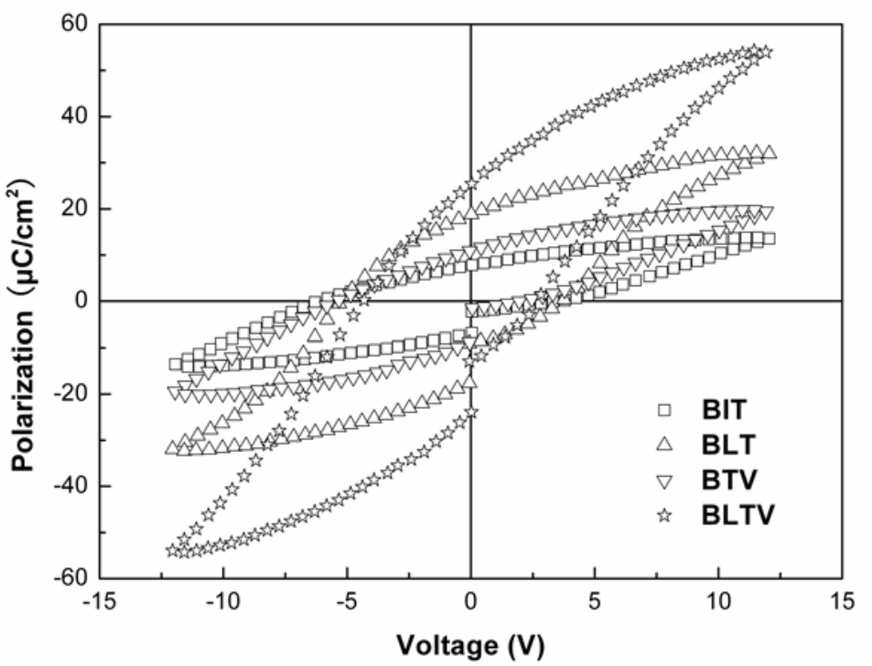

Fig. 4. Polarization-voltage (*P-V*) hysteresis loops of the BIT, BLT, BTV and BLTV thin films at the voltage of 12 V

Figure 5 illustrates the fatigue characteristics of these thin films. The test was performed at room temperature using 12 V, 100 kHz bipolar square pulses. From the figure we can see that, as the switching cycles increase, the normalized P_r (the P_r to the initial polarization) of the BLT, BTV and BLTV films decreases silghtly, while that of the BIT film decreases greatly. The P_r of the BIT, BLT, BTV and BLTV films decreases by 24%, 14%, 16% and 10% respectively after 10^{10} cycles.

The strongest fatigue endurance for the BLTV film and good fatigue property for the BLT and BTV films after La^{3+} and V^{5+} substitution are due to the decrease of the defects, such as oxygen vacancies. For BLSF materials, some oxygen vacancies and Bi vacancies are generated unavoidably because of the volatilization of Bi during the annealing processes under high temperatures (Yuan & Or, 2006). The reaction mechanism is as follow:

$$2Bi^{3+} + 3O^{2-} \leftrightarrow Bi_2O_3 + 2v_{Bi}^{'''} + 3v_o^{\cdot\cdot} \tag{2}$$

where $v_o^{\cdot\cdot}$ is the oxygen vacancy with valence of +2, and $v_{Bi}^{'''}$ is the Bi vacancy with valence of -3. The oxygen vacancies are the hole trappers and act as the space charges. And they cause strong domain pinning with repetitive switching cycles, which deteriorate the properties of the ferroelectric films (Park & Chadi, 1998). Better chemical stability of the perovskite layers against oxygen vacancies after substitution of some *A*-site Bi atoms for La

atoms is helpful to the fatigue behavior (Kang et al., 1999). For the BTV and BLTV films, V^{5+} substitution for Ti^{4+} and a decrease in Bi content are conducted simultaneously to maintain the charge neutrality, as indicated by the equation of composition ($Bi_{4-x/3}Ti_{3-x}V_xO_{12}$ and $Bi_{3.25-x/3}La_{0.75}Ti_{3-x}V_xO_{12}$). Furthermore, the substitution of the *B*-site Ti^{4+} for the donor-type V^{5+} can suppress the generation of oxygen vacancies due to the charge neutrality restriction (Sun et al., 2006). The reaction mechanisms are as follows:

$$V_2O_5 \leftrightarrow 2V_{\dot{T}i} + 5O_O + 2e' \tag{3}$$

$$\frac{1}{2}O_2 + v_o^{\cdot\cdot} + 2e' \leftrightarrow O_O \tag{4}$$

$$Bi + v_{Bi}''' + 3V_{\dot{T}i} \leftrightarrow Bi_{Bi} + 3V_{Ti} \tag{5}$$

where $V_{\dot{T}i}$ is the V ion with +1 effective charge at the Ti site, V_{Ti} is the V at the Ti, O_O is oxide in the lattice, Bi_{Bi} is Bi in the lattice, and e is the compensatory charge. Thus, v_{Bi}''', the tervalent negative electric center, is neutralized by $V_{\dot{T}i}$, and the oxygen vacancies are suppressed by the higher-valentcation substitution. So the substitution of *A*-site La^{3+} and *B*-site V^{5+} in BIT thin film can improve the properties of the ferroelectric thin film effectively. The BLT and BTV thin films show good fatigue properties.

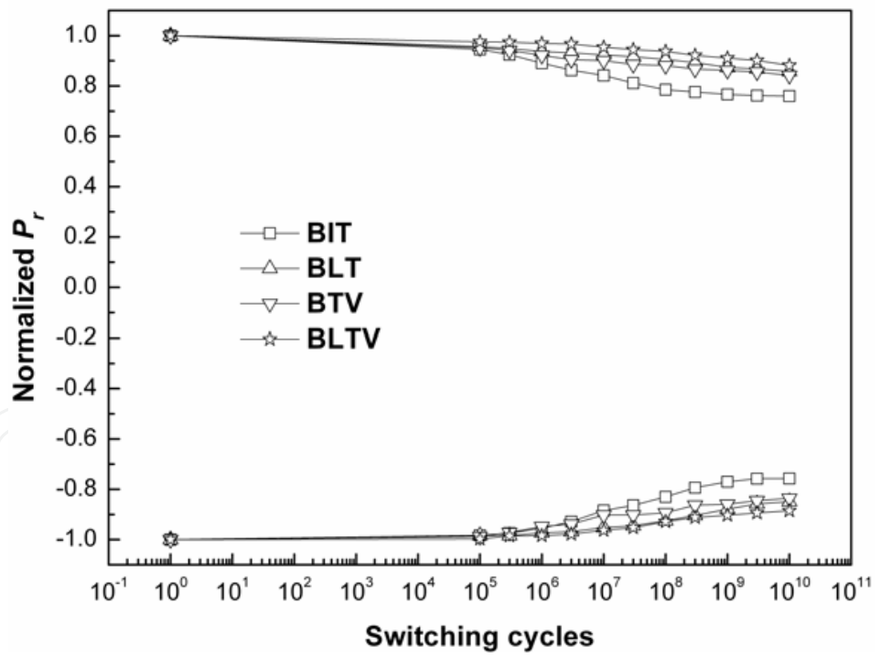

Fig. 5. Fatigue characteristics of the BIT, BLT, BTV and BLTV thin films

The volatile Bi is partly substituted for La, and there are still Bi and oxygen vacancies. There are small amounts of V^{5+} substitution in the present BLTV film, which could avoid more charge defects caused by excessive V^{5+} substitution according to equation (3). The decrease of oxygen vacancies still follows the proposed equation (4) in the BLTV film except for the effect of La^{3+} substitution. The decrease and suppression of oxygen vacancies are enhanced

by simultaneous substitutions of La^{3+} and V^{5+} in the BLTV film. Thus, cosubstitution of La^{3+} and V^{5+} in the BLTV film results in its excellent fatigue property.

The dc leakage current is usually one of the most concerned factors for NvFRAM application of ferroelectric thin films, because of its direct relation to power consumption and function failure of devices (Araujo et al., 1990). Therefore leakage current measuremnts are a crucial part of any electrical characterization. During the measurement, the dc voltage over a range of 0-5 V was applied with a step of 0.05 V, and a delay time of 10 s between each step to ensure the collected data of steady state. The leakage current characteristics of current density (*J*) versus electric field (*E*) for these thin films at room temperature are shown in Fig. 6. The leakage current density increases gradually at low electric field, but generally in the order of 10^{-9}-10^{-8} A/cm^2 for the BLTV film, 10^{-8}-10^{-7} A/cm^2 for the BLT and BTV films, and 10^{-6}-10^{-5} A/cm^2 for the BIT film below 100 kV/cm. The leakage current density of the BLT and BTV films is smaller than that of the BIT film, and the BLTV film acquires the smallest leakage current density.

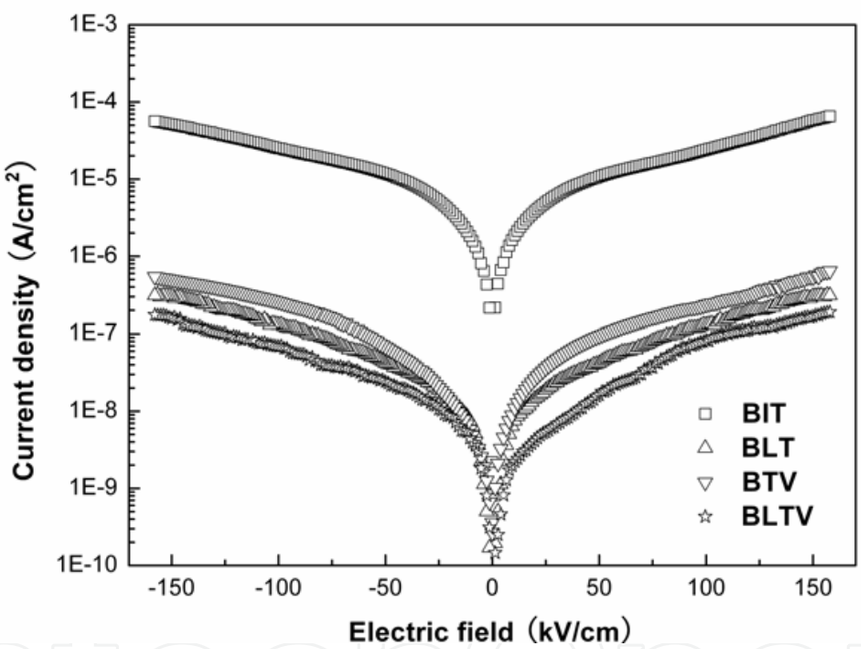

Fig. 6. Electric field dependence of leakage current density for the BIT, BLT, BTV and BLTV thin films

For further study of the effect of La^{3+} and V^{5+} cosubstitution, the leakage current behaviors for the BIT and BLTV films were measured at various temperatures from 20 to 150°C in Fig. 7. The mechanisms of leakage currents are closely related to the temperature for the thermally assisted conduction process. There is a systematic increase in leakage current density with the increase in temperature for both of the films, but the leakage current density for the BIT film increases faster with the increase of the voltage and temperature. Figs 7 (c) and (d) show the plots of log *J* versus log *E* of the films in the temperature range from 20 to 150°C. In the low electric field region, the leakage current shows an ohmic behavior with the slope of log *J*/log *E* being about 1. The linear region extends up to a onset voltage, at which the space charges start dominating the conduction process. The onset voltage decreases with the increase of the temperature, which is seen from the figures. In the

high electric field region, the slope is varying from 2.16 to 2.30 for the BLTV film with the increase of the temperature, while 2.28 to 2.72 for the BIT film, which agrees with the space charge limited current (SCLC) leakage mechanism for both of the films. The larger slop for the BIT film could be caused by more thermally excited electrons from trap levels in the film (Chaudhun & Krupanidhi, 2005). Both electrons and oxygen vacancies domain the space charge mechanism. At low temperatures, oxygen vacancies somehow do not respond to the high electric field, and the highly mobile electrons are the major charge carriers of the current. However, oxygen vacancies play a significant role in the space charge mechanism at high temperatures (Bhattacharyya et al., 2002). From Figs 7 (c) and (d), we can see that the leakage current density increases in three order of magnitude for the BIT film in the high electric field at 150^{o}C(when the temperature was increased from 20 to 150^{o}C), while increases in less than one order of magnitude for the BLTV film. For there are more oxygen vacancies in the BIT film, the leakage current density for the film increases drastically in the high electric field at the high temperature. Therefore, the improved leakage current property is also attributed to the decrease and suppression of oxygen vacancies after La^{3+} and V^{5+} substitution in the thin films.

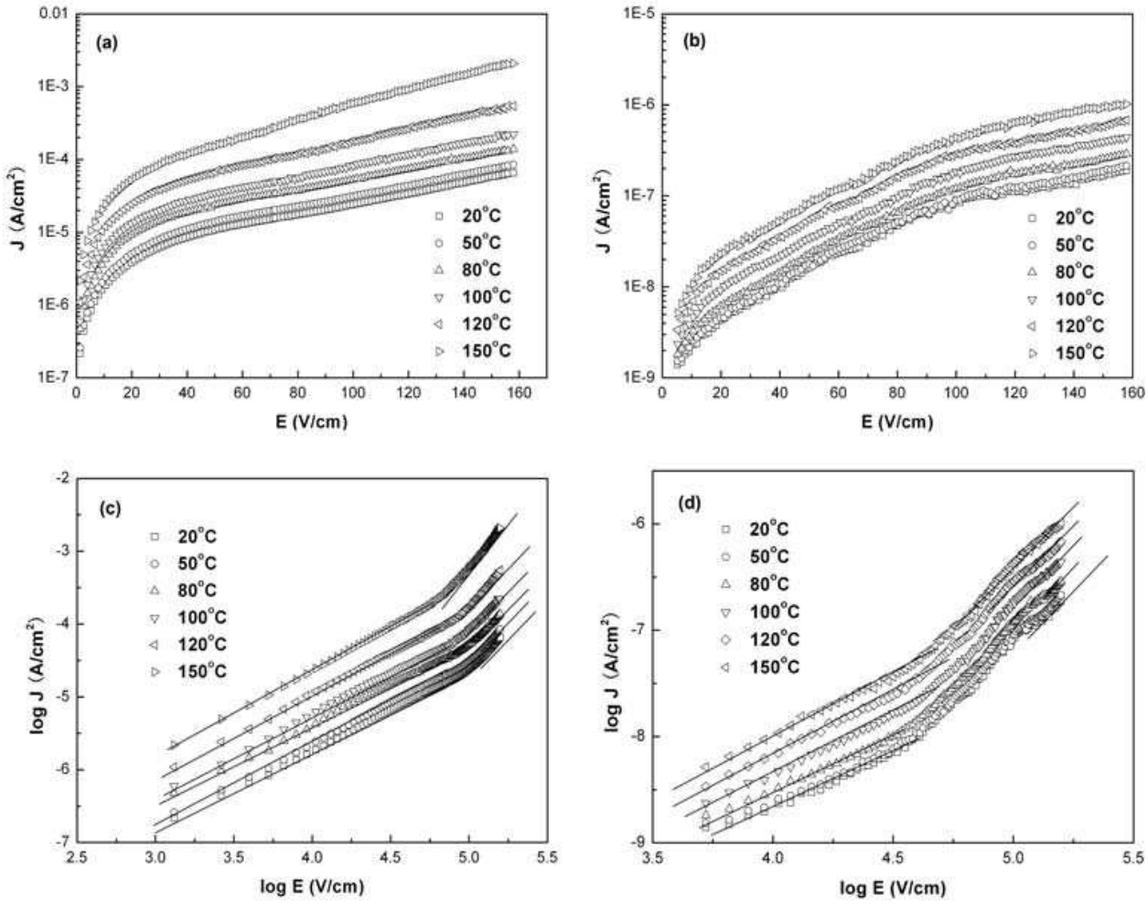

Fig. 7. Leakage current characteristics at the temperature range from 20 to 150^{o}C: J-E plots for the (a) BIT and (b) BLTV thin films; the log J vs log E plots for the (c) BIT and (d) BLTV thin films

3.3 The Effect of V content in BLTV

To acquire the optimal content of V substitutition, $Bi_{3.25-x/3}La_{0.75}Ti_{3-x}V_xO_{12}$ were prepared with different content of V substitutition (x: 0-8%) by sol-gel processes.

The XRD patterns of the BLT, BLTV(x=1%, 3%, 5%, 8%) thin films deposited on the $Pt/TiO_2/SiO_2/p$-Si(100) substrates are shown in Fig. 8. It can be seen that increasing V content do not destroy their crystal structure and all the films are the layered perovskite structure. The BLT film without V substitution exhibits higher intensity of (006) peak. The intensity of this peak decreases with V content increasing from 0 to 0.05, but increases again when V content increasing to 0.08. The volume fraction of c-axis-oriented grains in $BLTV_x$ (0-8%) films calculated according to equation (1) is 31.7, 21.5, 16.9, 20.8 and 39.3 respectively. Thus, the BLTV(3%) film shows the least degree of c-axis orientation.

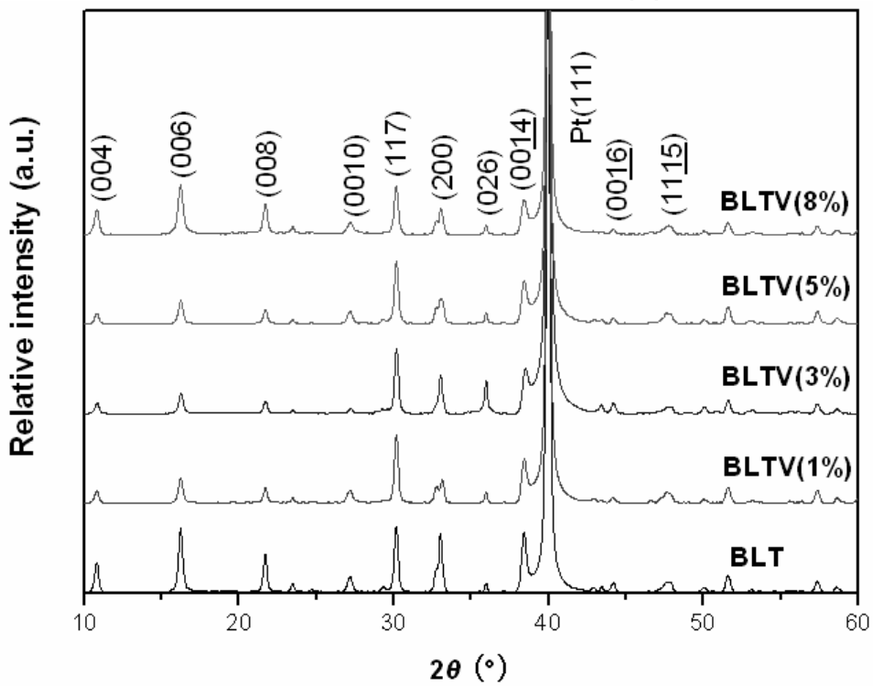

Fig. 8. XRD patterns of the BLTV(x: 0-8%) thin films deposited on the $Pt/TiO_2/SiO_2/p$-Si(100) substrates

Figure 9 shows the FE-SEM surface and cross-section morphologies of the BLTV(x: 0-8%) thin films. All the films show dense microstructure without any crack. From the surface morphologies, it can be seen that the BLT film is mainly composed of fine rod-like and plate-like grains. The rod-like grains increase but the plate-like grains decrease with V content increasing, and there are most rod-like grains when V content is 3% and 5%. Whereas, plate-like grains increase again when V content increasing to 8%. The result of FE-SEM surface morphologies agrees with that of the XRD patterns discussed above.

The Raman spectra for these BLTV(x: 0-8%) thin films were investigated in the Raman frequency shift range of 100-1000 cm^{-1} as presented in Fig. 10. The 852 cm^{-1} mode is a pure stretching of TiO_6 octahedron, Raman shift for BLTV(1%), BLTV(3%), BLTV(5%) and BLTV(8%) thin films is 851, 850, 850 and 848 cm^{-1} respectively at this mode. There are two obvious peaks between 600 and 800 cm^{-1} mode for BLTV(8%) thin film, which indicates a great increase of the structural distortion and a great decrease in O_h symmetry of TiO_6 octahedron.

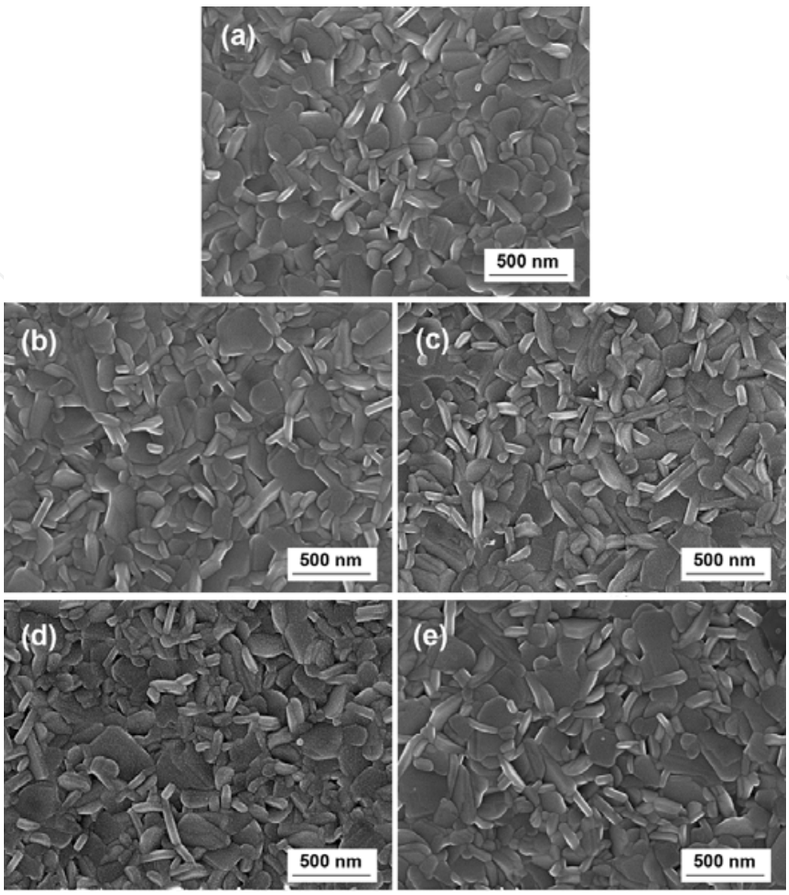

Fig. 9. FE-SEM surface morphologies of the BLTV(*x*: 0-8%) thin films: (a) BLT, (b) BLTV(1%), (c) BLTV(3%), (d) BLTV(5%) and (e) BLTV(8%)

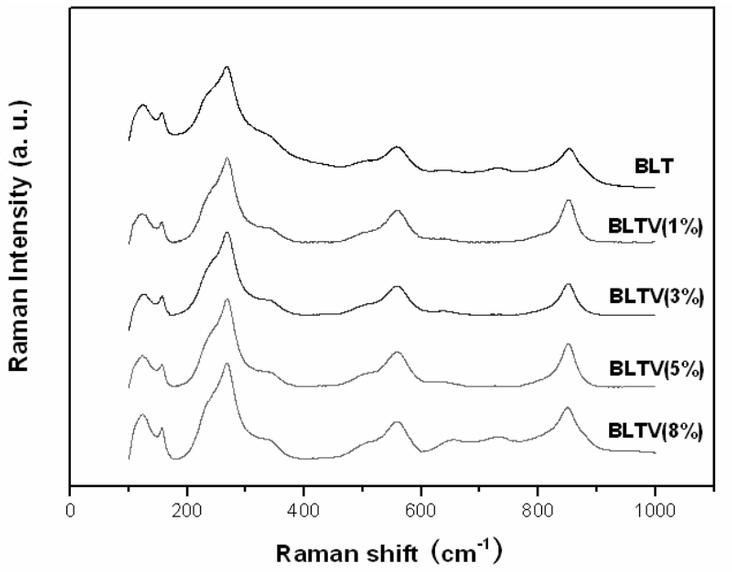

Fig. 10. Raman spectra of the BLTV(*x*: 0-8%) thin films

Figure 11 shows the *P-V* curves of these BLTV(*x*: 0-8%) thin film capacitors at a voltage of 12 V. All these thin films show well-saturated hystersis loops. With increasing of substitution content, P_r increases. In the range x>3%, P_r decreases with increasing V content. When x=8%, P_r becomes lower than that of BLT and the squareness of the hystersis loop is degraded as well.

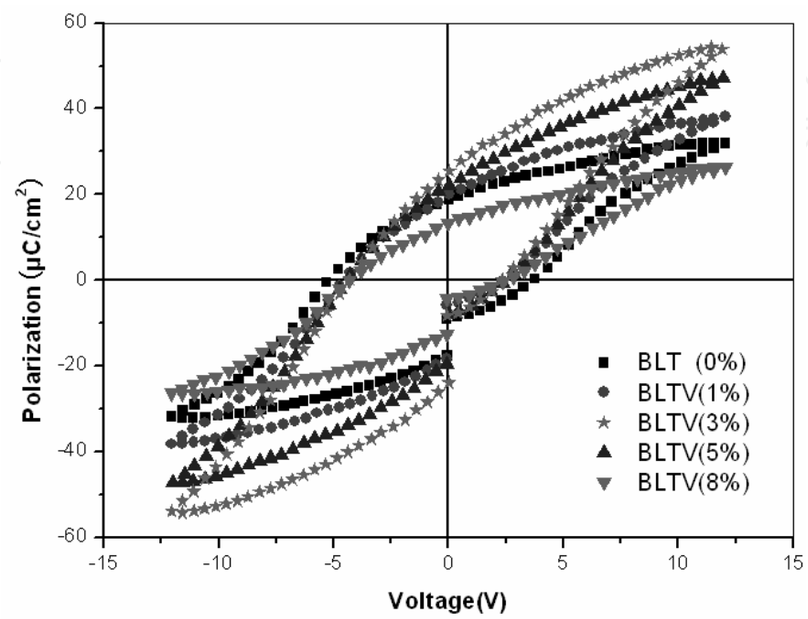

Fig. 11. Polarization-voltage (*P-V*) hysteresis loops of the BLTV(*x*: 0-8%) thin films at the voltage of 12 V

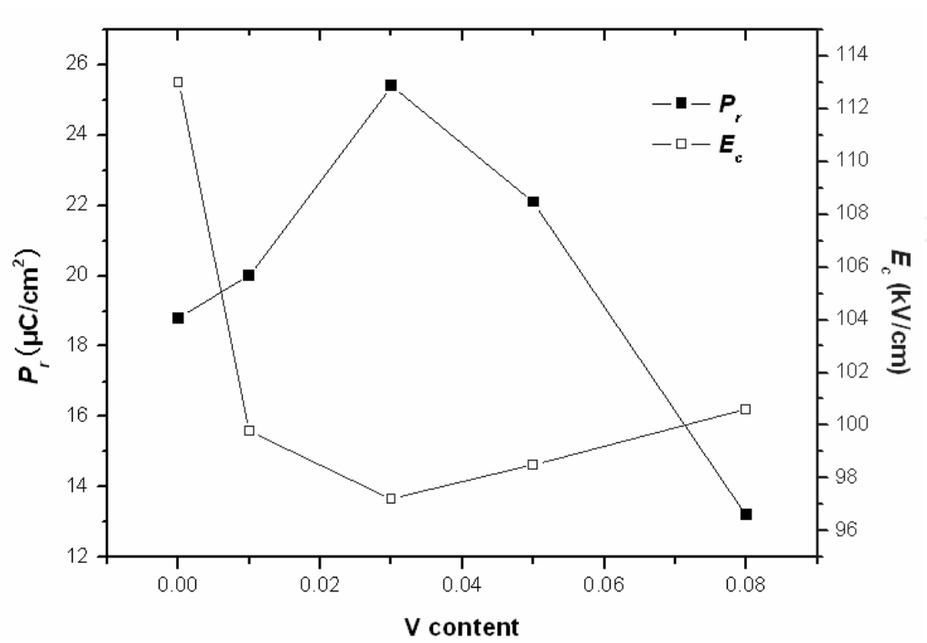

Fig. 12. P_r and E_c of the BLTV(*x*: 0-8%) thin films as functions of the V content

Figure 12 summarizes the variation in the P_r and E_c against the V content in the BLTV(x: 0-8%) thin films. The P_r values under the voltage of 12 V were 18.8, 20.1, 25.4, 22.1 and 13.2 μC/cm², respectively, for x = 0, 1%, 3%, 5%, 8%. The BLTV(3%) thin film gets the largest P_r for its least degree of c-axis orientation. On the other hand, as hybridization is essential to ferroelectricity, the increase of hybridization may increase the polarization. Thus the increase of Ti-O hybridization inside TiO_6 of the BLTV(3%) thin film results in its excellent ferroelectric properties. After the substitution content is above 5%, P_r begins to decrease, this is because of a limited solution of V ion in BLTV thin films. The great increase of the structural distortion results in a great decrease of ferroelectric properties.

Figure 13 illustrates the fatigue characteristics of these BLTV(x: 0-8%) thin films. With increasing of substitution content, the fatigue property is improved. In the range x>3%, the fatigue property is worsened with increasing V content. Small amounts of V^{5+} substitution can suppress the generation of oxygen vacancies due to the charge neutrality restriction, but excessive V^{5+} substitution will cause more charge defects which worsen the fatigue property.

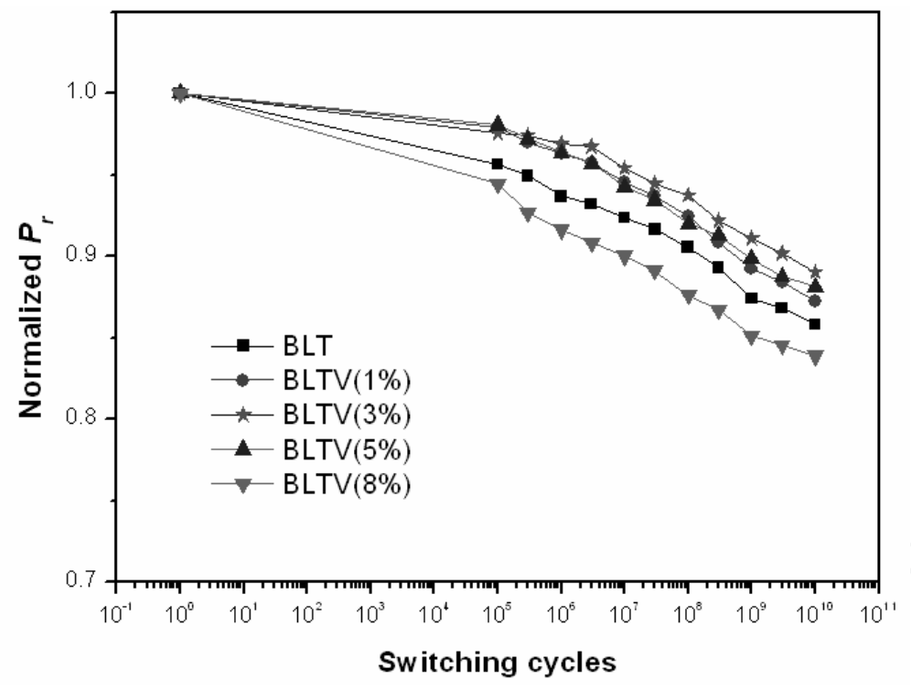

Fig. 13. Fatigue characteristics of the BLTV(x: 0-8%) thin films

4. Conclusion

In conclusion, BIT, BLT, BTV and BLTV thin films were fabricated on the Pt/TiO_2/SiO_2/p-Si(100) substrates by sol-gel processes. The microstructures and electrical properties of these films after substitution of La^{3+} and V^{5+} were investigated. The X-ray diffraction patterns indicate the BLTV thin film shows randomly oriented with fine rod-like grains revealed

from the FE-SEM surface and cross-section morphologies. Raman spectra show the *A*-site La^{3+} substitution exerts influence on Ti^{4+} ions in *B* sites of the BIT thin film, TiO_6 (or VO_6) symmetry decreases and Ti-O (or V-O) hybridization increase for V^{5+} substitution. Either *A*-site La^{3+} or *B*-site V^{5+} substitution can improve the P_r value for the BIT thin film, but only the BLT and BLTV film capacitors are characterized by well-saturated *P-V* curves at an applied voltage of 12 V. The BLTV thin film shows the largest $2P_r$ of 50.8 μC/cm² with small $2E_c$ of 194 kV/cm among these films. For the BLTV thin film, the fatigue test exhibits the strongest fatigue endurance up to 10^{10} cycles and the leakage current density is generally in the order of 10^{-9}-10^{-8} A/cm² below 100 kV/cm at room temperature while increasing in less than one order of magnitude at the temperature range from 20 to 150°C. To acquire the optimal concentration of V substitutition, BLTV were prepared with different concentration of V substitutition (x: 0-8%). The remanent polarization and fatigue properties first increase then decrease with increasing of V content. BLTV(3%) thin film exhibits excellent ferroelectric property and the strongest fatigue endurance up to 10^{10} cycles. When V content increases to 8%, the properties decrease due to slightly large distortion of crystal lattice and charge defects caused by excessive V substitution. The excellent properties of the BLTV thin film are attributed to the effective decrease or suppression of oxygen vacancies after La^{3+} and V^{5+} substitution in the thin film.

5. References

Araujo, C. A.; Mcnillan, L. D.; Melnick, B. M.; Cuchiaro, J. D. & Scott, J. F. (1990). Ferroelectric memories. *Ferroelectrics,* Vol. 104, No. 1, pp. 241-256, ISSN 0015-0193

Bae, J. C.; Kim, S. S.; Choi, E. K.; Song, T. K.; Kim, W. J. & Lee, Y. I. (2005). Ferroelectric properties of lanthanum-doped bismuth titanate thin films grown by a sol–gel method. *Thin Solid Films,* Vol. 472, No. 1-2, pp. 90-95, ISSN 0040-6090

Bhattacharyya, S.; Laha, A. & Krupanidhi, S. B. (2002). Analysis of leakage current conduction phenomenon in thin $SrBi_2Ta_2O_9$ films grown by excimer laser ablation. *J. Appl. Phys.,* Vol. 91, No. 7, pp. 4543-4548, ISSN 0021-8979

Chaudhuri, A. R. & Krupanidhi, S. B. (2005). dc leakage behavior in vanadium-doped bismuth titanate thin films. *J. Appl. Phys.,* Vol. 98, No. 9, 094112, ISSN 0021-8979

Chen, M.; Liu, Z. L.; Wang, Y.; Wang, C. C.; Yang, X. S. & Yao, K. L. (2004). Ferroelectric properties of Pr_6O_{11}-doped $Bi_4Ti_3O_{12}$. *Solid State Communications,* Vol. 130, No. 11, pp. 735-739, ISSN 0038-1098

Chen, M.; Liu, Z. L.; Wang, Y.; Wang, C. C.; Yang, X. S. & Yao, K. L. (2004). Ferroelectric properties and microstructures of Sm-doped $Bi_4Ti_3O_{12}$ ceramics. *Physica B,* Vol. 352, No. 1-4, pp. 61-65, ISSN 0921-4526

Choi, E. K.; Kim, S. S.; Kim, J. K.; Bae, J. C.; Kim, W. J.; Lee, Y. I. & Song, T. K. (2004). Effects of donor ion doping on the orientation and ferroelectric properties of bismuth titanate thin films. *Jpn. J. Appl. Phys.,* Vol. 43, pp. 237-241, ISSN 0021-4922

Chon, U.; Kim, K. B.; Jang, H. M. & Yi, G. C. (2001). Fatigue-free samarium-modified bismuth titanate ($Bi_{4-x}Sm_xTi_3O_{12}$) film capacitors having large spontaneous polarizations. *Appl. Phys. Lett.,* Vol. 79, No. 19, pp. 3137-3139, ISSN 0003-6951

Chon, U.; Jang, H. M.; Kim, M. G. & Chang C. H. (2002). Layered perovskites with giant spontaneous polarizations for nonvolatile memories. *Phys. Rev. Lett.,* Vol. 89, No. 8, 087601, ISSN 0031-9007

Chon, U.; Shim, J. S. & Jang, H. M. (2003). Ferroelectric properties and crystal structure of praseodymium-modified bismuth titanate. *J. Appl. Phys.,* Vol. 93, No. 8, pp. 4769-4775, ISSN 0021-8979

Cohen, R. E. (1992). Origin of ferroelectricity in perovskite oxides. *Nature,* Vol. 358, pp. 136-138, ISSN 0028-0836

Fuierer, P. & Li, B. (2002). Nonepitaxial orientation in sol–gel bismuth titanate films. *J. Am. Ceram. Soc.,* Vol. 85, No. 2, pp. 299-304, ISSN 1551-2916

Garg, A.; Barber, Z. H.; Dawber, M.; Scott, J. F.; Snedden, A. & Lightfoot, P. (2003). Orientation dependence of ferroelectric properties of pulsed-laser-ablated $Bi_{4-x}Nd_xTi_3O_{12}$ films. *Appl. Phys. Lett.,* Vol. 83, No. 12, pp. 2414-2416, ISSN 0003-6951

Hou, F.; Shen, M. R. & Cao, W. W. (2005). Ferroelectric properties of neodymium-doped $Bi_4Ti_3O_{12}$ thin films crystallized in different environments. *Thin Solid Films,* Vol. 471, No. 1-2, pp. 35-39, ISSN 0040-6090

Kim, J. K.; Kim, J.; Song, T. K. & Kim, S. S. (2002). Effects of niobium doping on microstructures and ferroelectric properties of bismuth titanate ferroelectric thin films. *Thin Solid Films,* Vol. 419, No. 1-2, pp. 225-229, ISSN 0040-6090

Kim, S. S.; Song, T. K., Kim, J. K. & Kim, J. (2002). Ferroelectric properties of vanadium-doped $Bi_4Ti_3O_{12}$ thin films deposited by a sol–gel method. *J. Appl. Phys.,* Vol. 92, No. 4, pp. 2213-2215, ISSN 0021-8979

Kim, S. S.; Bae, J. C. & Kim, W. J. (2005). Fabrication and ferroelectric studies of (Bi, $Gd)_4Ti_3O_{12}$ thin films grown on $Pt/Ti/SiO_2/Si$ and p-type Si substrates. *Journal of Crystal Growth,* Vol. 274, No. 3-4, pp. 394-401, ISSN 0022-0248

Lee, J. K.; Kim, C. H.; Suh, H. S. & Hong, K. S. (2002). Correlation between internal stress and ferroelectric fatigeue in $Bi_{4-x}La_xT_3O_{12}$ thin films. *Appl. Phys. Lett.,* Vol. 80, No. 19, pp. 3593-3595, ISSN 0003-6951

Lee, H. N.; Hesse, D.; Zakharov, N. & Gösele, U. (2002). Ferroelectric $Bi_{3.25}La_{0.75}Ti_3O_{12}$ Films of Uniform a-Axis Orientation on Silicon Substrates. *Science,* Vol. 296, No. 5575, pp. 2006-2009, ISSN 0036-8075

Li, J.; Yu, J.; Peng, G.; Wang, Y. B. & Zhou, W. L. (2007). The influence of the thickness of TiO_2 seeding layer on structural and electrical properties of $Bi_{3.15}Nd_{0.85}Ti_3O_{12}$ thin films. *J. Phys. D: Appl. Phys.,* Vol. 40, pp. 3788-3792, ISSN 0022-3727

Lu, C. J.; Qiao, Y.; Qi, Y. J.; Chen, X. Q. & Zhu, J. S. (2005). Large anisotropy of ferroelectric and dielectric properties for $Bi_{3.15}Nd_{0.85}Ti_3O_{12}$ thin films deposited on $Pt/Ti/SiO_2/Si$. *Appl. Phys. Lett.,* Vol. 87, No. 22, 222901, ISSN 0003-6951

Matsuda, H.; Ito, S. & Lijima, T. (2003). Design and ferroelectric properties of polar-axis-oriented polycrystalline $Bi_{4-x}Pr_xTi_3O_{12}$ thick films on Ir/Si substrates. *Appl. Phys. Lett.,* Vol. 83, No. 24, pp. 5023-5025, ISSN 0003-6951

Mao, X. Y.; He, J. H., Zhu, J. & Chen, X. B. (2006). Structural, ferroelectric, and dielectric properties of vanadium-doped $Bi_{4-x/3}Ti_{3-x}V_xO_{12}$. *J. Appl. Phys.,* Vol. 100, No. 4, 044104, ISSN 0021-8979

Park, B. H., Kang, B. S., Bu, S. D., Noh, T. W.; Lee, J. & Jo, W. (1999). Lanthanum-substituted bismuth titanate for use in non-volatile memories. *Nature,* Vol. 401, pp. 682-684, ISSN 0028-0836

Park, C. H. & Chadi D. J. (1998). Microscopic study of oxygen-vacancy defects in ferroelectric perovskites. *Phys. Rev. B,* Vol. 57, R13961, ISSN 1098-0121

Paz De Araujo, C. A., Cuchiaro, J. D., McMillan, L. D., Scott, M. C. & Scott, J. F. (1995). Fatigue-free ferroelectric capacitors with platinum electrodes. *Nature,* Vol. 374, pp. 627-629, ISSN 0028-0836

Ramesh, R.; Luther, K.; Wilkens, B.; Hart, D. L.; Wang, E. & Trascon, J. M. (1990). Epitaxial growth of ferroelectric bismuth titanate thin films by pulsed laser deposition. *Appl. Phys. Lett.,* Vol.57, No. 15, pp.1505-1507, ISSN 0003-6951

Scott, J. F. & Paz De Araujo, C. A. (1989). Ferroelectric memories. *Science,* Vol. 246, No. 4936, pp. 1400-1405, ISSN 0036-8075

Shulman, H. S.; Damjanovic, D. & Setter, N. (2000). Niobium doping and dielectric anomalies in bismuth titanate. *J. Am. Ceram. Soc.,* Vol. 83, No. 3, pp. 528-532, ISSN 1551-2916

Simoes, A. Z.; Pianno, R. F. C.; Ries, A.; Varela, J. A. & Longo, E. (2006). a-b axis-oriented lanthanum doped $Bi_4Ti_3O_{12}$ thin films grown on a TiO_2 buffer layer. *J. Appl. Phys.,* Vol. 100, No. 8, 084106, ISSN 0021-8979

Sun, H.; Zhu, J., Fang, H. & Chen, X. B. (2006). Large remnant polarization and excellent fatigue property of vanadium-doped $SrBi_4Ti_4O_{15}$ thin films. *J. Appl. Phys.,* Vol. 100, No. 7, 074102, ISSN 0021-8979

Takenaka, T. & Sanaka, K. (1980). Grain orientation and electrical properties of hot-forged $Bi_4Ti_3O_{12}$ ceramics. *Jpn. J. Appl. Phys.,* Vol. 19, pp. 31-39, ISSN 0021-4922

Uchida, H.; Yoshikawa, H.; Okada, I.; Matsuda, H.; Lijima, T.; Watanabe, T.; Kojima, T. & Funakubo, H. (2002). Approach for enhanced polarization of polycrystalline bismuth titanate films by Nd^{3+}/V^{5+} cosubstitution. *Appl. Phys. Lett.,* Vol. 81, No.12, pp. 2229-2231, ISSN 0003-6951

Wang, X. S. & Ishiwara, H. (2003). Polarization enhancement and coercive field reduction in W- and Mo-doped $Bi_{3.35}La_{0.75}Ti_3O_{12}$ thin films. *Appl. Phys. Lett.,* Vol. 82, No. 15, pp. 2479-2481, ISSN 0003-6951

Watanabe, T.; Funakubo, H.; Osada, M.; Uchida, H. & Okada, I. (2005). The effects of neodymium content and site occupancy on spontaneous polarization of epitaxial $(Bi_{4-x}Nd_x)Ti_3O_{12}$ films. *J. Appl. Phys.,* Vol. 98, No. 2, 024110, ISSN 0021-8979

Wu, D.; Li, A. D.; Zhu, T.; Li, Z. F.; Liu, Z. G. & Ming, N. B. (2001). Processing- and composition-dependent characteristics of chemical solution deposited $Bi_{4-x}La_xTi_3O_{12}$ thin films. *J. Mater. Res.,* Vol. 16, No. 5, pp. 1325-1332, ISSN 0884-2914

Yau, C. Y.; Palan, R.; Tran, K. & Buchanan, R. C. (2005). Mechanism of polarization enhancement in La-doped $Bi_4T_3O_{12}$ films. *Appl. Phys. Lett.,* Vol. 86, No. 3, 032907, ISSN 0003-6951

Yuan, G. L. & Or, S. W. (2006). Enhanced piezoelectric and pyroelectric effects in single-phase multiferroic $Bi_{1-x}Nd_xFeO_3$ (x = 0–0.15) ceramics. *Appl. Phys. Lett.,* Vol. 88, No. 6, 062905, ISSN 0003-6951

Zhu, J.; Chen, X. B.; Zhang, Z. P. & Shen, J. C. (2005). Raman and X-ray photoelectron scattering study of lanthanum-doped strontium bismuth titanate. *Acta. Mater.,* Vol. 53, No. 11, pp. 3155-3162, ISSN 1359-6454

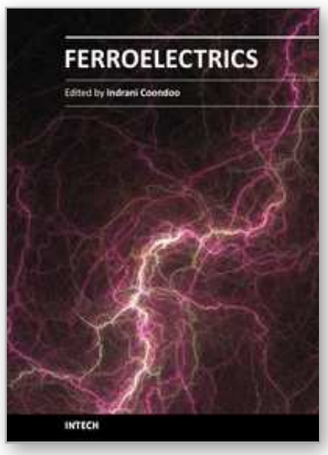

Ferroelectrics

Edited by Dr Indrani Coondoo

ISBN 978-953-307-439-9
Hard cover, 450 pages
Publisher InTech
Published online 14, December, 2010
Published in print edition December, 2010

Ferroelectric materials exhibit a wide spectrum of functional properties, including switchable polarization, piezoelectricity, high non-linear optical activity, pyroelectricity, and non-linear dielectric behaviour. These properties are crucial for application in electronic devices such as sensors, microactuators, infrared detectors, microwave phase filters and, non-volatile memories. This unique combination of properties of ferroelectric materials has attracted researchers and engineers for a long time. This book reviews a wide range of diverse topics related to the phenomenon of ferroelectricity (in the bulk as well as thin film form) and provides a forum for scientists, engineers, and students working in this field. The present book containing 24 chapters is a result of contributions of experts from international scientific community working in different aspects of ferroelectricity related to experimental and theoretical work aimed at the understanding of ferroelectricity and their utilization in devices. It provides an up-to-date insightful coverage to the recent advances in the synthesis, characterization, functional properties and potential device applications in specialized areas.

InTech Europe
University Campus STeP Ri
Slavka Krautzeka 83/A
51000 Rijeka, Croatia
Phone: +385 (51) 770 447
Fax: +385 (51) 686 166
www.intechopen.com

InTech China
Unit 405, Office Block, Hotel Equatorial Shanghai
No.65, Yan An Road (West), Shanghai, 200040, China
中国上海市延安西路65号上海国际贵都大饭店办公楼405单元
Phone: +86-21-62489820
Fax: +86-21-62489821

IntechOpen